Unconventional Thermally Activated Indirect to Direct Radiative Recombination of Electrons and Holes in Tin Disulfide Two- Dimensional van der Waals Material

Bhaskar, Prashant; Achtstein, Alexander W.; Vermeulen, Martien; Siebbeles, Laurens

DOI
10.1021/acs.jpcc.9b01842

Publication date
2019

Document Version
Final published version

Published in
The Journal of Physical Chemistry C

THE JOURNAL OF PHYSICAL CHEMISTRY C

Article

Cite This: J. Phys. Chem. C XXXX, XXX, XXX−XXX

pubs.acs.org/JPCC

Unconventional Thermally Activated Indirect to Direct Radiative Recombination of Electrons and Holes in Tin Disulfide Two-Dimensional van der Waals Material

Prashant Bhaskar,*[,†] Alexander W. Achtstein,[‡] Martien J. W. Vermeulen,[†] and Laurens D. A. Siebbeles*[,†]

[†]Optoelectronic Materials Section, Department of Chemical Engineering, Delft University of Technology, Van der Maasweg 9, 2629 HZ Delft, The Netherlands

[‡]Institute of Optics and Atomic Physics, Technical University of Berlin, Strasse des 17. Juni 135, 10623 Berlin, Germany

ABSTRACT: Tin disulfide (SnS_2) is a two-dimensional semiconducting van der Waals material with an indirect band gap. We measured the mobility and recombination dynamics of charge carriers as a function of temperature and charge density. Excess electrons and holes were generated by pulsed irradiation with 3 MeV electrons. The charge carriers were probed by time-resolved microwave conductivity measurements. The mobility and decay pathways of the charge carriers were determined by a global kinetic rate equation model including decay of charges by recombination and trapping. We found high mobilities for electrons and holes near 100 $cm^2\ V^{-1}\ s^{-1}$. The mobility decreases at higher temperature, which is typical for bandlike transport. The second-order recombination rate constant is found to be thermally activated with an activation energy close to the energy difference of the direct and indirect band gap of SnS_2. We demonstrate that the radiative recombination is reaction-limited and takes place via the Γ-point after thermal excitation of electrons from the *M*-point to the Γ-point, while a phonon emission-related recombination between the indirect band gap (*M*-point electrons and Γ-point holes) has no relevant contribution to the population decay. The observed effects result in an unusual increase of radiative electron−hole recombination constant with temperature.

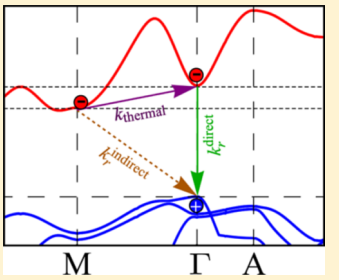

INTRODUCTION

Two-dimensional layered materials are of interest because of their intriguing optical and electronic properties and promising prospects for application in optoelectronic devices.[1−7] Beyond graphene, black phosphorus and transition-metal dichalcogenides have been studied extensively.[8−13] Among other emerging metal dichalcogenide materials, tin disulfide (SnS_2) currently attracts attention for (opto)electronic,[14−18] (thermo)electrical,[19,20] photovoltaic,[21] water splitting,[22] and photocatalytical applications.[23]

Bulk SnS_2 is a semiconductor with an indirect band gap of 2.29 eV and a direct band gap of 2.44 eV.[18,24] It consists of layers of hexagonally attached tin and sulfur atoms that are stacked together by weak van der Waals forces. Unlike other transition-metal dichalcogenides, monolayers and few layers of SnS_2 also exhibit an indirect band gap.[19,25] However, upon application of biaxial tensile strain,[26] an indirect to direct band gap transition can be induced.

The mobility and decay pathways of charge carriers play an important role in (opto)electronic devices. According to a theoretical first-principles (i.e., ab initio without adjustable parameters) study, the electron and hole mobilities in a monolayer of SnS_2 are as high as 756, and 187 $cm^2\ V^{-1}\ s^{-1}$, respectively.[19] As mentioned in ref 19, the high charge mobility in SnS_2 as compared to other 2D materials is due to the lower effective mass and lower deformation potential constant (thus longer electron−phonon scattering time). For a monolayer of SnS_2, electron mobilities of 50 and 230 $cm^2\ V^{-1}\ s^{-1}$ have been measured, while values of 1.5 and 20 $cm^2\ V^{-1}\ s^{-1}$ were found for samples of 10 and 120 nm thickness, respectively.[25,27] For bulk SnS_2 electron, dc mobilities in the range 15−50 $cm^2\ V^{-1}\ s^{-1}$ have been found,[14,28] and a combined electron and hole ac mobility of 150 $cm^2\ V^{-1}\ s^{-1}$ has been published.[17]

Figure 1 illustrates the band structure of SnS_2 electron band energies versus their quasi-momentum (*k*-value), as obtained from density functional theory (DFT) calculations described in the Methods section below. Quantitative results from detailed DFT and GW calculations can be found elsewhere.[19,26,29] The maximum of the valence band is near the Γ-point (*k* is zero), while according to DFT, the minimum in the conduction band is at the *M*-point (*k* is nonzero) and according the GW calculations it is at the *L*-point (*k* is nonzero).[25,26] The different *k*-values at the valence band maximum and the conduction band minimum cause SnS_2 to be an indirect band gap semiconductor.[16,25,29] Further details of the definition of the abovementioned *k* values can be found elsewhere.[25,26] Recombination of electrons and holes via the indirect band gap (indicated by the orange arrow in Figure 1) occurs via a phonon-assisted process to conserve momentum. It is also possible that the electron is first thermally excited from the *M*-

Received: February 26, 2019
Revised: April 10, 2019
Published: April 17, 2019

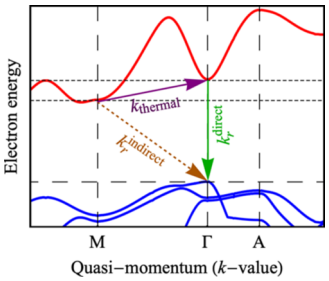

Figure 1. Illustration of the band structure of SnS_2 obtained from a DFT calculation. The purple arrow indicates thermal excitation of an electron from the indirect band gap to the direct band gap, orange and green arrows indicate electron−hole recombination via the indirect and direct band gap.

point to the Γ-point in the conduction band (rate $k_{thermal}$ indicated by the purple arrow in Figure 1), followed by radiative recombination (green arrow in Figure 1). The latter process is expected to occur with an activation energy equal to the energetic difference (0.15 eV) between the *M*-point to the Γ-point in the conduction band.

To our knowledge, the charge carrier mobility in SnS_2 has been reported for room temperature only, and no studies on the mechanism of decay of electrons and holes have been published. The aim of this work involves characterization of the mobility and recombination pathways of charge carriers in bulk SnS_2. Electrons and holes were generated by irradiation of the sample with 3 MeV electron pulses, and their decay dynamics was probed by contactless microwave conductivity measurements at various temperatures. According to theoretical analysis of the magnitude and decay kinetics of the conductivity, electrons and holes have a mobility near 100 $cm^2 V^{-1} s^{-1}$ and predominantly decay via recombination after thermal electron excitation from the *M*-point to the Γ-point in the conduction band.

METHODS

Transient Conductivity. Thin flakes of SnS_2 (2H phase) were procured from HQ Graphene (Groningen, The Netherlands) with 99.995% purity and used without further treatment. The yellowish translucent flakes of SnS_2 were filled into a polyetheretherketone (PEEK) sample holder with a groove of 1 mm along the direction of high-energy electron irradiation, analogous to our previous study on Te.[30] The flakes were tightly pressed to fill the groove entirely. The sample holder was inserted into a copper waveguide cell suitable to perform microwave conductivity studies in the K_a-band (28−37 GHz), similar to previous studies.[30−32]

Electrons and holes were generated in the sample via irradiation with 3 MeV electron pulses from a van de Graaff electron accelerator. The 3 MeV electrons lose part of their energy by impact-ionization in the sample, leading to a uniform spatial distribution of electron−hole pairs. The stopping range of the incident 3 MeV electrons exceeds the 1 mm sample length, and therefore, they pass through the sample so that charge neutrality is maintained. Successive irradiation did not affect the measured microwave conductivity, which implies the absence of effects of radiation damage.

The radiation dose D_{SnS_2} deposited in SnS_2 by the 3 MeV electrons was obtained from $D_{SnS_2} = D_{Bz}(N_{e,SnS_2}\rho_{SnS_2}M_{Bz}/N_{e,Bz}\rho_{Bz}M_{SnS_2})$, where D_{Bz} = 530 J m^{-3} nC^{-1} is the reference dose absorbed by benzene (Bz), and *N*, ρ, and *M* are the number of electrons per molecule, mass density, and molecular mass of SnS_2 or benzene, respectively. The mass density of SnS_2 and benzene are 4.5 and 0.88 g cm^{-3}, respectively. The density of electron−hole pairs generated in SnS_2 per unit time during the 3 MeV electron pulse is $G_{pulse} = D_{SnS_2}/(E_p t_{pulse})$, where E_p is the pair-formation energy and t_{pulse} is the pulse duration. For semiconductors, the pair formation energy for high-energy electron irradiation can be estimated according to an empirical formula provided by Alig et al.[33] which is given by $E_p = 2.73E_g + b$, where b = 0.5 eV and E_g = 2.29 eV is the band gap of SnS_2 in the 2H phase.[18,34]

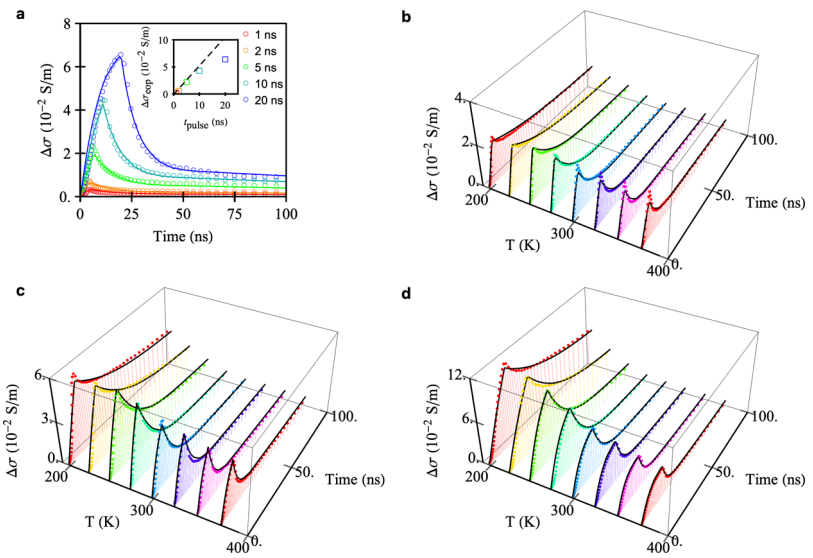

Figure 2. Transient microwave conductivity of charge carriers in SnS_2 at room temperature obtained for various pulse durations at T = 298 K (a) and for various temperatures from 198 to 373 K for 5 (b) 10 (c) and 20 ns (d) pulse durations. The dotted curves are the experimental conductivity traces, and the drawn curves were obtained from theoretical modeling. The inset in (a) shows the end-of-pulse conductivity, $\Delta\sigma_{cop}$, as a function of pulse duration t_{pulse}.

DOI: 10.1021/acs.jpcc.9b01842
J. Phys. Chem. C XXXX, XXX, XXX−XXX

The generated charge carriers absorb a part, $\Delta P(t)$, of the incident microwave power P, which is related to the conductivity $\Delta\sigma(t)$ by $\Delta P(t)/P = -AB\Delta\sigma(t)$, where A and B are sensitivity factors; see refs.[35,36] The factor A accounts for the effect of microwave cell dimensions and the dielectric constant of the sample. The factor B accounts for the effects due to heterogeneity of the sample resulting from the layers of SnS_2 and the PEEK sample holder. This leads to an effective dielectric constant that can be described by[35,37,38]

$$\varepsilon_{**} = \varepsilon_*' - j\varepsilon_*'' = d\left[\sum_i \frac{d_i}{\varepsilon_i' - j\varepsilon_i''}\right]^{-1} \quad (1)$$

In the above equation, ε_* is the effective dielectric constant due to the stacked layers with real and imaginary dielectric constants ε_i' and ε_i'' with layer thickness d_i, and total thickness d, while $j^2 = -1$. A picture illustrating the effect of the layers in eq 1 can be found in ref 35.

DFT Calculations. For illustrative purpose, the band structure of SnS_2 was calculated using the Amsterdam DFT program (ADF-BAND).[39−41] The calculation was done using a DZP (double zeta and one polarization) basis set and the Perdew−Burke−Ernzerhof generalized gradient approximation density functional. Relativistic spin−orbit coupling was taken into account.

RESULTS AND DISCUSSION

Time-Dependent Microwave Conductivity Due to Charge Carriers. Figure 2 shows the transient conductivity of electrons and holes for different durations t_{pulse} of the 3 MeV electron pulse and sample temperatures T. The inset in Figure 2a shows the end-of-pulse conductivities $\Delta\sigma_{cop}$ for t_{pulse} ranging from 1 to 20 ns. The sublinear increase of $\Delta\sigma_{cop}$ with t_{pulse} for longer pulse duration is an indication of higher-order recombination during the pulse at higher charge carrier density. Figure 2b−d shows the transient conductivities for t_{pulse} equal to 5, 10, and 20 ns in the temperature range of 198−373 K. It is observed that the decay of the conductivity becomes faster as the temperature increases.

Theoretical Modeling. The formation and decay dynamics of the electrons and holes can be described by the following coupled differential equations

$$\frac{dn_1(t)}{dt} = G_{pulse}\phi_1 - k_1 n_1(t) - k_r n_1(t) n_2(t) \quad (2)$$

$$\frac{dn_2(t)}{dt} = G_{pulse}\phi_2 - k_2 n_2(t) - k_r n_1(t) n_2(t) \quad (3)$$

In eqs 2 and 3, $n_1(t)$ and $n_2(t)$ are interchangeable electron and hole densities, as the experiment cannot distinguish which corresponds to electrons and which to holes. The densities generated during the 3 MeV electron pulse with generation rate G is determined to be $(8.4 \pm 1.1) \times 10^{15}$ cm^{-3} ns^{-1}, as described in the Methods section. The term $G_{pulse} = G[\Theta(t) - \Theta(t - t_{pulse})]$ with Θ the Heaviside function is non-zero during the electron pulse only. The factors ϕ_1 and ϕ_2 are the initial yields of charges of type 1 and 2, respectively, accounting for the survival fraction of charges from geminate recombination and trapping on timescales shorter than t_{pulse}. The rate constants k_1 and k_2 account for the first-order decay of charges to traps. The rate-constant k_r accounts for second-order (radiative) recombination of electrons and holes. The relation between the transient microwave conductivity $\Delta\sigma(t)$, the transient densities of charges $n_1(t)$ and $n_2(t)$, and the charge mobilities μ_1 and μ_2 is given by

$$\Delta\sigma(t) = e[\mu_1 n_1(t) + \mu_2 n_2(t)] \quad (4)$$

Equations 2−4 were globally fitted to the experimental data for a data set consisting of varying t_{pulse} and T with μ_1, μ_2, k_1, k_2, k_r, ϕ_1, and ϕ_2 as fit parameters. Figure 2 shows that the theoretical fits reproduce the experimental results very well.

Mobility and Initial Yield of Charges. Figure 3 shows the temperature-dependent mobility of charges of type 1 and 2

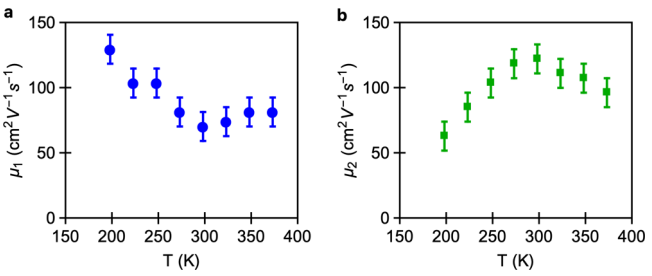

Figure 3. Temperature-dependent mobility for charges of type 1 and 2 in panel (a,b), respectively.

obtained from the fit. For the charges of type 1, the mobility μ_1 decreases with temperature, which is typical for bandlike transport with increased electron−phonon scattering reducing the mobility at higher temperature.

The mobility μ_2 of charges of type 2 first increases with temperature up to 300 K and then decreases at higher temperature. The initial increase could be due to scattering of charge carriers on static defects in SnS_2, as increasing thermal energy charge carriers can surpass static defects more easily. With further increase in temperature, the reduction of the mobility could be due to increasing relevance of charge carrier-phonon scattering, limiting the mobility. It is not unexpected that the phonon scattering has a different impact on electrons and holes, as for example, the deformation potential constants for both charge carriers can be significantly different.[42]

Figure 4 shows that the initial yield of type 1 charges, ϕ_1, remains constant with t_{pulse}. This can be due to the presence of

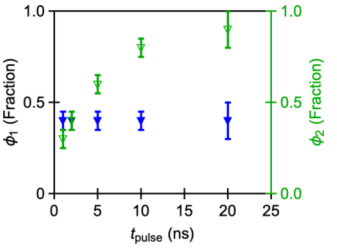

Figure 4. Initial yield of charges of type 1 and 2 as a function of pulse duration.

shallow traps, where a thermal equilibrium between trapping and de-trapping of charges appears. In such a case, the rate equation for density of trapped charges at equilibrium at a particular temperature can be written as

$$\frac{dn_1^{free}}{dt} = -k_1^{trap} n_1^{free} + k_1^{detrap} n_1^{trapped} = 0 \quad (5)$$

DOI: 10.1021/acs.jpcc.9b01842
J. Phys. Chem. C XXXX, XXX, XXX−XXX

where n_1^{free}, $n_1^{trapped}$, k_1^{trap}, and k_1^{detrap} are the free charge density, trapped charge density, trapping rate, and de-trapping rate for charges of type 1, at short times during the pulse t_{pulse}. According to eq 5, at equilibrium, the ratio of free charge density and trapped charge density is equal to the ratio k_1^{detrap}/k_1^{trap}. For shallow traps, these rates may be sufficiently high so that equilibrium is reached on a timescale much shorter than t_{pulse} and ϕ_1 reaches the equilibrium value. Furthermore, it was found that ϕ_1 is virtually temperature-independent, implying a merely constant ratio k_1^{detrap}/k_1^{trap}. From this, we infer that the energetic depth of the shallow traps is less than 15 meV, which is the thermal energy corresponding to the lowest temperature of 198 K used in the experiments. On the other hand, it is observed that initial yield of charges of type 2, ϕ_2, increases with t_{pulse}. This can be due to enhanced filling and eventual saturation of traps, as the pulse duration (and thus the charge density) increases. The yield ϕ_2 is also found to be temperature-independent, which is ascribed to shallow traps with energy less than the lowest thermal energy of 15 meV in the experiments.

Charge Carrier Recombination and Decay. The second-order (radiative) recombination constant k_r found from the fits of the theoretical model described above increases strongly with temperature; see Figure 5a. The thermal activation can be understood as follows: as can be seen in Figure 1, recombination via the indirect band gap of SnS_2 corresponds to a transition of an electron from the M-point in the conduction band to the Γ-point in the valence band. This transition involves a change of momentum of the electron. To conserve total momentum, the transition must be accompanied by phonon emission or absorption. The alternative recombination process occurs by thermal excitation of an electron from the M-point to the Γ-point in the conduction band and subsequent radiative recombination with the hole; see Figure 1.[25] The recombination rate constant associated with this pathway is thermally activated because it requires excitation of an electron from the M-point to the Γ-point. The activation energy, ΔE = 0.15 eV,[18,24] is the difference between the direct and indirect band gap of SnS_2.

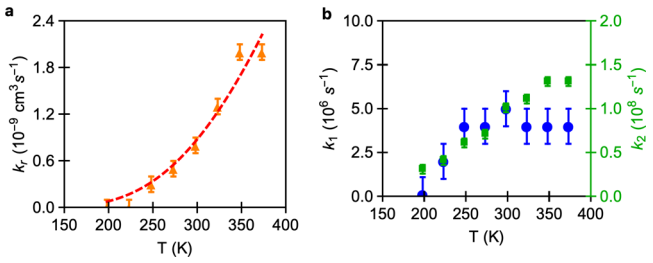

Figure 5. (a) Temperature-dependent second-order recombination rate constant k_r obtained from fitting the theoretical model (see eqs 2−4) to the experimental conductivity data (triangular markers). The dashed line is a fit of eq 6 to the data. (b) Temperature dependence of trapping rate constants k_1 (blue) and k_2 (green) for charges of types 1 and 2.

The total recombination rate is the sum of the rates for the transition via the indirect band gap, $k_r^{indirect}$, and the direct band gap, k_r^{direct}, which according to the work of Hall is given by[43]

$$k_r = k_r^{indirect} + k_r^{direct} \exp\left(\frac{-\Delta E}{k_B T}\right) \quad (6)$$

In eq 6, $k_r^{indirect} = A_i \coth(\theta/2T)$ and $k_r^{direct} = A_d T^{-3/2}$, where the prefactor A_i and A_d are temperature-independent,[43−45] θ is the Debye temperature (calculated to be 137 K for SnS_2[19]), and k_B is the Boltzmann constant. We fitted eq 6 to the data points in Figure 5a, yielding the dashed curve with $k_r^{indirect} < 10^{-12}$ cm^3 s^{-1} and $k_r^{direct} = (2.3 \pm 0.2) \times 10^{-7}$ cm^3 s^{-1}. Note that the temperature dependence of the second term in eq 6 is dominated by the exponential part and is merely affected by the weak temperature dependence of k_r^{direct}. With these values, the recombination rate via the direct band gap is found to be at least 2 orders of magnitude higher than via the indirect band gap. Hence, electrons−hole recombination occurs mainly via thermal excitation of an electron to the Γ-point and subsequent radiative decay. So far, we have considered reaction-limited recombination only. In general, second-order recombination can also be a diffusion-limited process with a Langevin recombination rate constant $k_r^{diff} = e(\mu_1 + \mu_2)/\varepsilon_0\varepsilon_r$,[46,47] where ε_0 and ε_r are the permittivity of vacuum and the dielectric constant of the material, respectively. Taking the room temperature value of $(\mu_1 + \mu_2)$ = 193 cm^2 V^{-1} s^{-1} and ε_r = 7.5,[48] the value of k_r^{diff} is calculated to be 5×10^{-7} cm^3 s^{-1}, which is more than 1 order of magnitude larger than the value of $(0.8 \pm 0.1) \times 10^{-9}$ cm^3 s^{-1} obtained from the experimental data. Hence, we conclude that recombination is not diffusion-limited, but occurs via the reaction-limited process with radiative decay at the Γ-point, as discussed above. We further remark that the thermally activated radiative rate constant leads to a decreasing radiative lifetime with increasing temperature, which may improve the radiative yield with temperature. As the increase of the first-order nonradiative rate constants in Figure 5b is weaker than the increase of the radiative rate for nearly all data points considered, a slight increase of the radiative yield or at least a near to constant behavior is expected. This sets the material system apart from conventional materials, which exhibits a strong decrease of the radiative yield with temperature, both because of increasing nonradiative processes and decreasing radiative rate.[30]

Next, we discuss the first-order nonradiative rates in Figure 5b. In case trapping is diffusion-controlled, the rate is proportional to the diffusion coefficient of the charge carrier, which is related to the mobility as $D = \mu k_B T/e$. The temperature dependence of the mobilities in Figure 3 then yields a much smaller thermal activation of D than the trapping rates in Figure 5b. Hence, trapping is not a diffusion-limited process. Apparently trapping occurs via a thermally activated reaction-limited pathway. The thermal activation can be due to the fact that the nuclear lattice undergoes a structural reorganization when a charge enters a trapping site. This is similar to polaron formation or Marcus charge transfer.[49]

CONCLUSIONS

At room temperature, the mobility of charge carriers of type 1 is 70 ± 12 cm^2 V^{-1} s^{-1} and that of the opposite charges is 123 ± 12 cm^2 V^{-1} s^{-1}. The observed decrease of the mobility at higher temperature is typical for a bandlike transport mechanism. Theoretical analysis of the charge carrier decay kinetics reveals that electron−hole recombination occurs by thermal promotion of electrons from the indirect to the direct band gap, followed by radiative recombination. Phonon-assisted recombination via the indirect band gap is found to be negligible. As we have demonstrated that the radiative recombination increases with temperature, the competing radiative and nonradiative processes can partially cancel out

DOI: 10.1021/acs.jpcc.9b01842
J. Phys. Chem. C XXXX, XXX, XXX−XXX

their combined temperature dependence, so that a slight increase or quasi-constant radiative yield for photon emission upon charge carrier recombination is expected, setting the system apart from conventional direct emitters.

AUTHOR INFORMATION

Corresponding Authors

*E-mail: p.bhaskar@tudelft.nl (P.B.).
*E-mail: l.d.a.siebbeles@tudelft.nl (L.D.A.S).

ORCID

Prashant Bhaskar: 0000-0002-5805-9756
Alexander W. Achtstein: 0000-0001-8343-408X
Laurens D. A. Siebbeles: 0000-0002-4812-7495

Notes

The authors declare no competing financial interest.

ACKNOWLEDGMENTS

P.B. and L.D.A.S. thank The Netherlands Organisation for Scientific Research (NWO) for financial support. A.W.A. acknowledges funding by DFG projects AC290/1-1 and AC290/2-1.

REFERENCES

(1) Zhou, X.; Zhang, Q.; Gan, L.; Li, H.; Xiong, J.; Zhai, T. Booming Development of Group IV-VI Semiconductors: Fresh Blood of 2D Family. *Adv. Sci.* **2016**, *3*, 1600177.

(2) Lin, Z.; et al. 2d Materials Advances: From Large Scale Synthesis and Controlled Heterostructures to Improved Characterization Techniques, Defects and Applications. *2D Mater.* **2016**, *3*, 042001.

(3) Castellanos-Gomez, A. Why All the Fuss About 2d Semiconductors? *Nat. Photon.* **2016**, *10*, 202−204.

(4) Mak, K. F.; Shan, J. Photonics and Optoelectronics of 2d Semiconductor Transition Metal Dichalcogenides. *Nat. Photon.* **2016**, *10*, 216.

(5) Niu, L.; Coleman, J. N.; Zhang, H.; Shin, H.; Chhowalla, M.; Zheng, Z. Production of Two-Dimensional Nanomaterials Via Liquid-Based Direct Exfoliation. *Small* **2016**, *12*, 272−293.

(6) Zhang, W.; Qixing, W.; Yu, C.; Zhuo, W.; Andrew, T. S. W. Van Der Waals Stacked 2d Layered Materials for Optoelectronics. *2D Mater* **2016**, *3*, 022001.

(7) Chen, Z.; Biscaras, J.; Shukla, A. Optimal Light Harvesting in 2d Semiconductor Heterostructures. *2D Mater.* **2017**, *4*, 025115.

(8) Ling, X.; Wang, H.; Huang, S.; Xia, F.; Dresselhaus, M. S. The Renaissance of Black Phosphorus. *Proc. Natl. Acad. Sci. U.S.A.* **2015**, *112*, 4523−4530.

(9) Choi, W.; Choudhary, N.; Han, G. H.; Park, J.; Akinwande, D.; Lee, Y. H. Recent Development of Two-Dimensional Transition Metal Dichalcogenides and Their Applications. *Mater. Today* **2017**, *20*, 116−130.

(10) Keyes, R. W. The Electrical Properties of Black Phosphorus. *Phys. Rev.* **1953**, *92*, 580−584.

(11) Ryder, C. R.; Wood, J. D.; Wells, S. A.; Hersam, M. C. Chemically Tailoring Semiconducting Two-Dimensional Transition Metal Dichalcogenides and Black Phosphorus. *ACS Nano* **2016**, *10*, 3900−3917.

(12) Zeng, Z.; Yin, Z.; Huang, X.; Li, H.; He, Q.; Lu, G.; Boey, F.; Zhang, H. Single-Layer Semiconducting Nanosheets: High-Yield Preparation and Device Fabrication. *Angew. Chem. Int. Ed.* **2011**, *50*, 11093−11097.

(13) Coleman, J. N.; et al. Two-Dimensional Nanosheets Produced by Liquid Exfoliation of Layered Materials. *Science* **2011**, *331*, 568−571.

(14) Shibata, T.; Muranushi, Y.; Miura, T.; Kishi, T. Photoconductive Properties of Single-Crystal 2h-Sns2. *J. Phys. Chem. Solids* **1990**, *51*, 1297−1300.

(15) Patil, S. G.; Tredgold, R. H. Electrical and Photoconductive Properties of Sns2 Crystals. *J. Phys. D: Appl. Phys.* **1971**, *4*, 718−722.

(16) Burton, L. A.; et al. Electronic and optical properties of single crystal SnS2: an earth-abundant disulfide photocatalyst. *J. Mater. Chem. A* **2016**, *4*, 1312−1318.

(17) Burton, L. A.; Colombara, D.; Abellon, R. D.; Grozema, F. C.; Peter, L. M.; Savenije, T. J.; Dennler, G.; Walsh, A. Synthesis, Characterization, and Electronic Structure of Single-Crystal SnS, Sn2S3, and SnS2. *Chem. Mater.* **2013**, *25*, 4908−4916.

(18) Powell, M. J.; Grant, A. J. The Effect of Pressure on the Optical-Absorption Edge in Sns2 and Snse2. *Nuovo Cimento B* **1977**, *38*, 486−495.

(19) Shafique, A.; Samad, A.; Shin, Y.-H. Ultra low lattice thermal conductivity and high carrier mobility of monolayer SnS2 and SnSe2: a first principles study. *Phys. Chem. Chem. Phys.* **2017**, *19*, 20677−20683.

(20) Szczech, J. R.; Higgins, J. M.; Jin, S. Enhancement of the Thermoelectric Properties in Nanoscale and Nanostructured Materials. *J. Mater. Chem.* **2011**, *21*, 4037−4055.

(21) Tan, F.; et al. Photovoltaic Effect of Tin Disulfide with Nanocrystalline/Amorphous Blended Phases. *Solid State Commun.* **2010**, *150*, 58−61.

(22) Sun, Y.; et al. Freestanding Tin Disulfide Single-Layers Realizing Efficient Visible-Light Water Splitting. *Angew. Chem. Int. Ed.* **2012**, *51*, 8727−8731.

(23) Zhuang, H. L.; Hennig, R. G. Theoretical Perspective of Photocatalytic Properties of Single-Layer Sns2. *Phys. Rev. B: Condens. Matter Mater. Phys.* **2013**, *88*, 115314.

(24) Green, N. J. B.; Pilling, M. J.; Pimblott, S. M.; Clifford, P. Stochastic models of diffusion-controlled ionic reactions-induced spurs. 2. Low-permittivity solvents. *J. Phys. Chem.* **1989**, *93*, 8025.

(25) Huang, Y.; et al. Tin Disulfide-An Emerging Layered Metal Dichalcogenide Semiconductor: Materials Properties and Device Characteristics. *ACS Nano* **2014**, *8*, 10743−10755.

(26) Ram, B.; Singh, A. K. Strain-Induced Indirect-to-Direct Band-Gap Transition in Bulk Sns_2. *Phys. Rev. B* **2017**, *95*, 075134.

(27) Song, H. S.; Li, S. L.; Gao, L.; Xu, Y.; Ueno, K.; Tang, J.; Cheng, Y. B.; Tsukagoshi, K. High-Performance Top-Gated Monolayer Sns2 Field-Effect Transistors and Their Integrated Logic Circuits. *Nanoscale* **2013**, *5*, 9666−9670.

(28) Gowers, J. P.; Lee, P. A. Mobility of Electrons in Sns2 Single Crystals. *Solid State Commun.* **1970**, *8*, 1447−1449.

(29) Gonzalez, J. M.; Oleynik, I. I. Layer-Dependent Properties of Sns_2 and $Snse_2$ Two-Dimensional Materials. *Phys. Rev. B* **2016**, *94*, 125443.

(30) Bhaskar, P.; Achtstein, A. W.; Vermeulen, M. J. W.; Siebbeles, L. D. A. Charge Mobility and Recombination Mechanisms in Tellurium Van Der Waals Solid. *J. Phys. Chem. C* **2019**, *123*, 841.

(31) Bhaskar, P.; Achtstein, A. W.; Diedenhofen, S. L.; Siebbeles, L. D. A. Mobility and Decay Dynamics of Charge Carriers in One-Dimensional Selenium Van Der Waals Solid. *J. Phys. Chem. C* **2017**, *121*, 18917−18921.

(32) Bhaskar, P.; Achtstein, A. W.; Vermeulen, M. J. W.; Siebbeles, L. D. A. Radiatively Dominated Charge Carrier Recombination in Black Phosphorus. *J. Phys. Chem. C* **2016**, *120*, 13836−13842.

(33) Alig, R. C.; Bloom, S.; Struck, C. W. Scattering by Ionization and Phonon Emission in Semiconductors. *Phys. Rev. B: Condens. Matter Mater. Phys.* **1980**, *22*, 5565−5582.

(34) Schmidt, W. F.; Allen, A. O. Free-Ion Yields in Sundry Irradiated Liquids. *J. Chem. Phys.* **1970**, *52*, 2345.

(35) Hoofman, R. J. O. M.; Siebbeles, L. D. A.; de Haas, M. P.; Hummel, A.; Bloor, D. Anisotropy of the Charge-Carrier Mobility in Polydiacetylene Crystals. *J. Chem. Phys.* **1998**, *109*, 1885−1893.

(36) Infelta, P. P.; de Haas, M. P.; Warman, J. M. The Study of the Transient Conductivity of Pulse Irradiated Dielectric Liquids on a Nanosecond Timescale Using Microwaves. *Radiat. Phys. Chem.* **1977**, *10*, 353−365.

(37) Warman, J. M.; de Haas, M. P.; Wentinck, H. M. The Study of Radiation Induced Conductivity Changes in Microheterogeneous

DOI: 10.1021/acs.jpcc.9b01842
J. Phys. Chem. C XXXX, XXX, XXX−XXX

Materials Using Microwaves. *Int. J. Radiat. Appl. Instrum. C Radiat. Phys. Chem.* **1989**, *34*, 581−586.
(38) Coelho, R. *Physics of Dielectrics for the Engineer/Roland Coelho*; Elsevier Scientific Pub. Co.: U.S., Canada, Elsevier/North-Holland: Amsterdam, New York, 1979.
(39) Baerends, E. J.; et al. *Adf2017, Scm, Theoretical Chemistry*; Vrije Universiteit: Amsterdam, the Netherlands, Https://Www.Scm.Com.
(40) te Velde, G.; Bickelhaupt, F. M.; Baerends, E. J.; Fonseca Guerra, C.; van Gisbergen, S. J. A.; Snijders, J. G.; Ziegler, T. Chemistry with Adf. *J. Comput. Chem.* **2001**, *22*, 931−967.
(41) Guerra, C. F.; Snijders, J. G.; te Velde, G.; Baerends, E. J. Towards an order- N DFT method. *Theor. Chem. Acc.* **1998**, *99*, 391−403.
(42) Yu, P. Y.; Cardona, M. *Fundamentals of Semiconductors*, 4 ed.; Springer, 2010.
(43) Hall, R. N. Recombination Processes in Semiconductors. *Proc. IEEE B, Electron. Commun. Eng.* **1959**, *106*, 923−931.
(44) Varshni, Y. P. Band-to-Band Radiative Recombination in Groups Iv, Vi, and Iii-V Semiconductors (I). *Phys. Status Solidi B* **1967**, *19*, 459−514.
(45) Landsberg, P. *Recombination in Semiconductors*; Cambridge University Press, 1991.
(46) Langevin, M. P. Recombinaison Et Mobilités Des Ions Dans Les Gaz. *Ann. Chim. Phys.* **1903**, *28*, 433−530.
(47) Lakhwani, G.; Rao, A.; Friend, R. H. Bimolecular Recombination in Organic Photovoltaics. *Annu. Rev. Phys. Chem.* **2014**, *65*, 557−581.
(48) Tin Disulfide (Sns_2) Optical Properties, Dielectric Constants. In *Non-Tetrahedrally Bonded Elements and Binary Compounds I*; Madelung, O., Rössler, U., Schulz, M., Eds.; Springer Berlin Heidelberg: Berlin, Heidelberg, 1998; pp 1−11.
(49) Schatz, G. C.; Ratner, M. A., *Quantum Mechanics in Chemistry*; Oxford University Press, 2002.

DOI: 10.1021/acs.jpcc.9b01842
J. Phys. Chem. C XXXX, XXX, XXX−XXX